Chemical Engineering Science 74 (2012) 27–37

Contents lists available at SciVerse ScienceDirect

Chemical Engineering Science

journal homepage: www.elsevier.com/locate/ces

Simulation study of an integrated methanol micro fuel processor and fuel cell system

Hsuan Chang [a,*], Shueh-Hen Cheng [b], Hao-Chang Chiang [a], Yih-Hang Chen [a], Yin-Yu Chang [a]

[a] Energy and Opto-Electronic Materials Research Center, Department of Chemical and Materials Engineering, Tamkang University, New Taipei City, Taiwan
[b] Department of Chemical and Materials Engineering, Tunghai University, Taichung, Taiwan

ARTICLE INFO

Article history:
Received 4 September 2011
Received in revised form
20 December 2011
Accepted 24 January 2012
Available online 7 February 2012

Keywords:
Chemical processes
Dynamic simulation
Energy
Microstructure
Process control
Fuel processor

ABSTRACT

The micro fabrication technology has facilitated the development of micro fuel processing systems to provide hydrogen for portable fuel cells. Methanol is a suitable liquid fuel for its high energy intensity and low operating temperature. In this study, a dynamic model for an integrated methanol micro fuel processing system and fuel cell is developed. The micro fuel processor employs plate-type micro devices. The steady state simulation analysis identifies the significant operating conditions for the micro FP/FC process, which are the feed flow rate and steam/carbon ratio of the steam reformer and the feed flow rate of the combustor. The dynamic simulation analysis compares the responds for the voltage change demand of PEMFC of three proposed control schemes, including the structures using double feedforward with double feedback control loops (CS1), double feedforward with single feedback control loops (CS2) and single feedforward with single feedback control loops (CS3). The CS2 plus a lag of 30 s is the best control structure.

1. Introduction

For portable applications, the proton exchange membrane fuel cell (PEMFC) is particularly attractive and promising (US DOE, 2000). Based on micro technology, micro scale fuel processors (FP) facilitate in-situ production of hydrogen-rich gases by reforming of liquid hydrocarbons for PEMFC applications. Compared to other fuels, methanol is the most appropriate and studied because of the low operation temperature, high hydrogen-carbon ratio, high energy density and ready availability. Shah et al. (2005) discussed the key issues in micro fuel processing, including miniaturization of system components, kinetics evaluation, water management, thermal management, dynamic control, fate of exhaust gases.

A methanol micro fuel processor involves several principal steps, such as combustion, steam reforming, carbon monoxide removal, fuel vaporization and heat exchange. Many researchers have focused on experimental and modeling studies of micro devices for these steps for performance demonstration or design investigation. Some investigated individual micro reactors, for example, Park et al. (2004) and Vahabi and Akbari (2009) studied methanol steam reformer and preferential oxidation reactor, respectively. Others investigated integrated micro units, such as reformer/combustor (Yoshida et al., 2006; Arzamendi et al., 2009) and preferential oxidation/heat exchanger (Delsman et al., 2004). Terazaki et al. (2005), Morse et al. (2007), Kolb et al. (2007) and Men et al. (2008) all have experimentally demonstrated the overall micro fuel processor system. Men et al. (2008) also studied the dynamics and control strategy of the system via simulation.

With these developments, a next research focus is on the integrated micro FP/FC system, which includes the fuel processor and the PEMFC. Men et al. (2008) and Kolb et al. (2009) reported the development work and experimental performance for complete micro FP/FC systems. The system performance and control structure are important issues and can be studied economically by simulation approach. This paper first presents a one dimensional dynamic model for an integrated methanol micro FP/FC system. The model is then utilized to investigate the effects of operating conditions and the performances of proposed control structures.

2. Process and modeling

In this section, the FP/FC process and the mathematical model are described.

The steam reforming reaction is highly endothermic. Thus, a combustor utilizing the hydrogen in the anode exhaust and external fuel is needed to provide the required energy input. For methanol-based fuel processing system, a CO clean up step must be included to meet the hydrogen input specification of a low temperature PEMFC. In this study, high degree of heat integration

* Corresponding author. Tel.: +886 2 26232094; fax: +886 2 26209887.
E-mail address: nhchang@mail.tku.edu.tw (H. Chang).

0009-2509/$ - see front matter © 2012 Elsevier Ltd. All rights reserved.
doi:10.1016/j.ces.2012.01.043

is embedded in the FP system design. However, the heat integration might be limited by practical considerations in device design. The integrated FP/FC process flow diagram is depicted in Fig. 1. The liquid methanol and water feed is vaporized in an evaporator (EV) before entering the steam reformer (SR). The hydrogen-rich gas product from SR is combined with an air stream and sent to a preferential oxidation unit (PrOx) together for reducing CO before providing as input to the fuel cell (FC). Another liquid methanol input is vaporized in an evaporative heat exchanger (HX-2) before feeding the combustor (CB), which is to support the endothermic steam reforming reaction. The process is thermally integrated to utilize the exhaust hydrogen from the anode of fuel cell and the exhaust flue gas from the combustor via several heat exchangers and integrated reactor/heat exchanger. For the PEMFC, hydrogen-rich gas and air inputs for anode and cathode are added after humidity adjustment with water, besides, cooling water is used for temperature control. In this study, the micro device chosen for reactor or heat exchanger is plate-type as shown in Fig. 2, which has two manifolds for input and output and many parallel rectangular channels. When used as reactors, the channel walls are coated with catalysts. The plate-type micro devices have been adopted by many researchers for fuel processor applications (Park et al., 2004; Delsman et al., 2005; Sohn et al., 2007; Chen et al., 2009). The unit specifications for this study are summarized in Tables 1 and 2. The system is designed for a power output of 50 W from the fuel cell. For the steam reforming, preferential oxidation and combustion reactors, the catalysts are assumed to be CuO/ZnO/Al_2O_3, Pt–Fe/Al_2O_3 and Pt/γ–Al_2O_3, respectively.

According to their functions, the mathematical models of the fuel processor units can be classified into three categories, i.e. reactor, single phase heat exchanger and heat exchanger with phase change. For the plate-type micro devices, the one dimensional models are developed. One common simplification of the unit models is the assumption of negligible pressure drop.

For reactors, the model is summarized in Appendix A. The model can be applied for single phase heat exchanger by removing the contents related to mass transfer and chemical reaction. The mass and energy balance equations are written, respectively, for the bulk gas in the micro channels and the solid walls, both with and without catalyst layer. Since the model is one dimensional, only variations in the flow direction (z-direction) are taken into account. The mass and thermal diffusions in the flow direction are neglected. For the bulk gas and the solid walls, the heat transfer and mass transfer (for solid wall with catalyst layer only) across the interface are determined using heat and mass transfer coefficients estimated from appropriate correlations for laminar flow in a duct. For the solid wall with catalyst layer, chemical reaction rates are calculated based on the reaction kinetics from Peppley et al. (1999), Korotkikh and Farrauto (2000) and Pasel et al. (2001) for SR, PrOx and CB, respectively.

For heat exchangers with phase change, a zero dimensional model (Llopis et al., 2007) is applied and is given in Appendix B. The heat exchanger is divided into sub-cooled liquid, vapor–liquid two phase and superheated vapor zones, as shown in Fig. 3. Solving the energy balance equations allows the determination of the volume of each zone and the intermediate and outlet stream temperatures. In the model, heat transfer coefficients are also determined by appropriate correlations.

For the PEMFC, a dynamic one dimensional model according to Golbert and Lewin (2004) is adopted and the model equations are referred to the paper. The mass balances of reactants are determined by the electrochemical reactions. The liquid and vapor water balances are determined by taking into account the reaction, condensation, vaporization and mass diffusion across the membrane. In the energy balance analysis, besides the heat of reaction, the heat transfers between solid and anode gas, cathode gas and cooling water are included. The model is dynamic for solid temperature and quasi-steady-state for all other variables. The model requires the voltage–current relationship from Nernst and Tafel equations (Bard and Faulkner, 2001).

The models are written using the commercial, equation-oriented process simulator Aspen Custom Modeler® and hence can easily be integrated with commercial process simulation packages. In Aspen Custom Modeler®, the overall process flowsheet can be built by connecting units and the model equations of

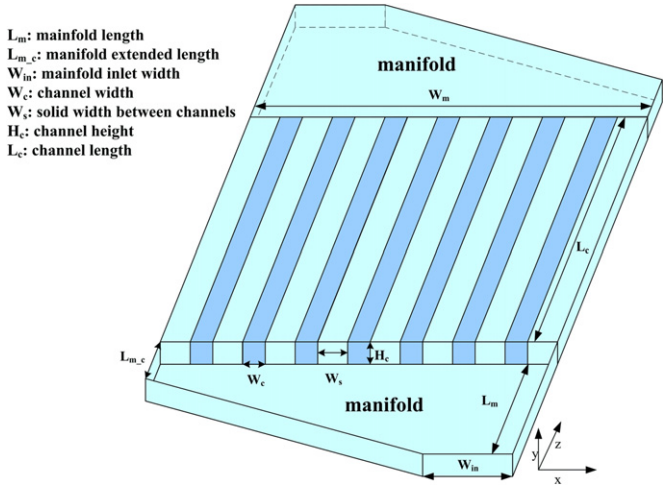

Fig. 2. Plate-type micro device.

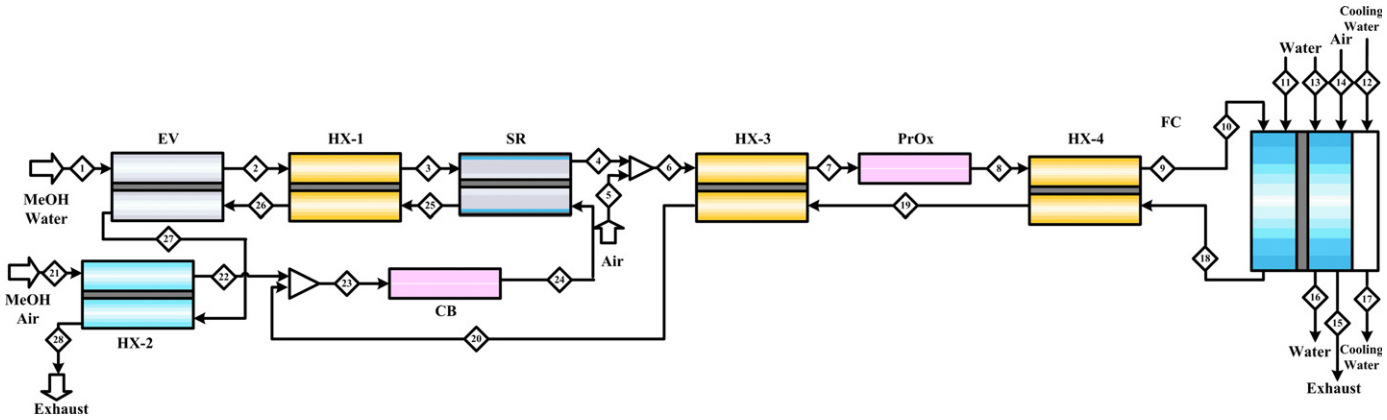

Fig. 1. Methanol fuel processor and fuel cell system.

Table 1
Specifications of fuel processor components.

Specifications	EV	CB	SR	PrOx
Catalyst	–	$Pt/\gamma-Al_2O_3$	$CuO/ZnO/Al_2O_3$	$Pt-Fe/Al_2O_3$
No. of reaction plates	42	35	80	35
No. of microchannels for each reaction plate	15	31	44	41
No. of heat exchange plates	42	–	80	–
No. of microchannels for each heat exchange plate	15	–	44	–
Height of microchannel (m)	2×10^{-4}	2×10^{-4}	2×10^{-4}	4.7×10^{-4}
Width of microchannel (m)	5×10^{-4}	5×10^{-4}	5×10^{-4}	5×10^{-4}
Length of microchannel (m)	4.5×10^{-2}	4.5×10^{-2}	4.5×10^{-2}	4.5×10^{-2}
Plate to plate spacing (m)	2×10^{-4}	2×10^{-4}	2×10^{-4}	4.7×10^{-4}
Channel to channel spacing (m)	2×10^{-4}	5×10^{-4}	5×10^{-4}	5×10^{-4}
Catalyst layer thickness (m)	–	3.3×10^{-5}	3.3×10^{-5}	5×10^{-6}
Device height (m)	1.76×10^{-2}	1.4×10^{-2}	3.56×10^{-2}	3.38×10^{-2}
Device width (m)	1.09×10^{-2}	2.2×10^{-2}	0.161	4.2×10^{-2}
Device length (m)	6.75×10^{-2}	6.75×10^{-2}	6.75×10^{-2}	6.75×10^{-2}
Device volume (m^3)	1.295×10^{-5}	2.079×10^{-5}	3.87×10^{-4}	9.58×10^{-5}
Specifications	**HX-1**	**HX-2**	**HX-3**	**HX-4**
Catalyst	–	–	–	–
No. of cold fluid plates	30	40	45	45
No. of microchannels for each cold fluid plate	18	7	44	40
No. of hot fluid plates	30	40	45	45
No. of microchannels for each hot fluid plate	18	7	44	40
Height of microchannel (m)	5×10^{-5}	2.5×10^{-4}	2×10^{-4}	2×10^{-4}
Width of microchannel (m)	5×10^{-5}	2.5×10^{-4}	2×10^{-4}	2×10^{-4}
Length of microchannel (m)	9.65×10^{-3}	9.65×10^{-3}	4.5×10^{-2}	4.5×10^{-2}
Channel to channel spacing (m)	5×10^{-5}	2.5×10^{-4}	2×10^{-4}	2×10^{-4}
Plate to plate spacing (m)	5×10^{-5}	2.5×10^{-4}	2×10^{-4}	2×10^{-4}
Device height (m)	6.02×10^{-3}	4.05×10^{-2}	3.64×10^{-2}	3.64×10^{-2}
Device width (m)	3.7×10^{-3}	7.5×10^{-3}	3.56×10^{-2}	3.24×10^{-2}
Device length (m)	1.45×10^{-2}	1.45×10^{-2}	6.75×10^{-2}	6.75×10^{-2}
Device volume (m^3)	3.23×10^{-7}	4.4×10^{-6}	8.75×10^{-5}	7.96×10^{-5}

Table 2
Specifications of fuel cell.

Specifications	FC	Anode	Cathode
Pressure (kPa)		150	150
Inlet Temperature (K)		333	343
Single MEA area (cm^2)	1		
No. of MEA	74		
Current density (A/cm^2)	1		
H_2 inflow (kg/s)		5.31×10^{-7}	–
O_2 inflow (kg/s)		–	2.42×10^{-5}
H_2O inflow (kg/s)		Saturated	Saturated
Cooling water flow rate (kg/s)	1.73×10^{-3}		
Cooling water temperature (K)	298		

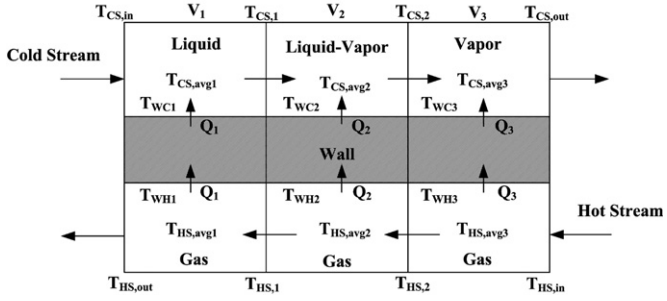

Fig. 3. Zone analysis for heat exchanger with phase change.

the overall process, which is developed by combining models of individual units, can be solved simultaneously. For each individual unit, given the information of device size and inlet fluids, the one dimensional profiles of temperature, concentration, mass flux and heat flux inside the unit can be solved. The reaction conversion and outlet fluid temperature and concentrations can also be obtained. For confirmation of the model correctness, simulation results of SR, PrOx and CB reactors have been verified with the experimental or simulation results reported by Park et al. (2004), Choi and Stenger (2004), Vahabi and Akbari (2009), Won et al. (2006) and Golbert and Lewin (2004).

3. Effects of operating conditions

The model is first utilized to analyze a base case. The specifications for the base case are: (1) the steam–carbon ratio, $(S/C)_{SR}$, for SR input is 1.3, (2) the oxygen–carbon monoxide ratio, $(O_2/CO)_{PrOx}$, for PrOx input is 1.63, (3) the air–carbon ratio, $(A/C)_{CB}$, for CB is 16.31, (4) the output power from fuel cell is 50 W. The simulation results for major units are listed in Table 3. The conversions of SR, PrOx and CB are all greater than 99% and the hydrogen utilization in FC is 76%. The CO concentration in the FC feed is 2.7 ppmv, which meets the desired upper limit of 10 ppmv. The methanol concentration in the CB exhaust gas is 93.2 ppmv, which should be lower than 200 ppmv. The voltage output from FC is 0.675 V.

To study the effects of operating conditions, they are individually varied from the base case values for simulation. For an integrated FP/FC, the important performance indexes include the methanol conversion in SR (X_{SR}), hydrogen production rate (F_{H2}), CO concentration in the hydrogen feed to the FC (C_{CO}), methanol concentration in the CB exhaust gas ($C_{MeOH,CB}$) and voltage output from the FC (V_{FC}). In this study, the current density pattern inside the FC is given and fixed. Thus, the voltage output directly reflects the power output of the FC (P_{FC}). The operating conditions examined are the feed flow rate ($F_{in,SR}$) and $(S/C)_{SR}$, the feed flow rate ($F_{in,CB}$) and $(A/C)_{CB}$, the $(O_2/CO)_{PrOx}$ and the cathode pressure

Table 3
Base case operation conditions and performance of major units.

Parameters	SR	PrOx	CB	FC
Temperature (K)	532–537	427–462	402–813	333–353
Pressure (kPa)	150	150	150	150
Feed flow rate (kg/s)	1.02671×10^{-5}	1.19723×10^{-5}	2.02×10^{-5}	5.31×10^{-7} (H_2); 2.42×10^{-5} (O_2)
Inlet composition	1.3 (S/C, molar)	1.63 (O_2/CO, molar)	16.3 (air/fuel, molar)	With saturated water
Conversion	99.3% (methanol)	99.98% (CO)	99.61% (methanol)	76% (H_2)
Product gas composition (mass fraction)	CH_3OH: 0.002 H_2O: 0.114 H_2: 0.106 CO: 0.0297 CO $_2$: 0.748	H_2O: 0.115 H_2: 0.083 O_2: 0.0104 CO: 5.2×10^{-6} (2.72 ppmv) CO_2: 0.643 N_2: 0.149	CH_3OH: 9.654×10^{-5} (93.2 ppmv) H_2O: 0.135 H_2: 1.451×10^{-5} O_2: 0.061 CO: 1.278×10^{-6} CO_2: 0.411 N_2: 0.428	
Production flow rate (kg/s)	1.096×10^{-6} (H_2)	1.062×10^{-6}	–	
Current density (A/cm^2)				1
Voltage (V)				0.675
Power (W)				50

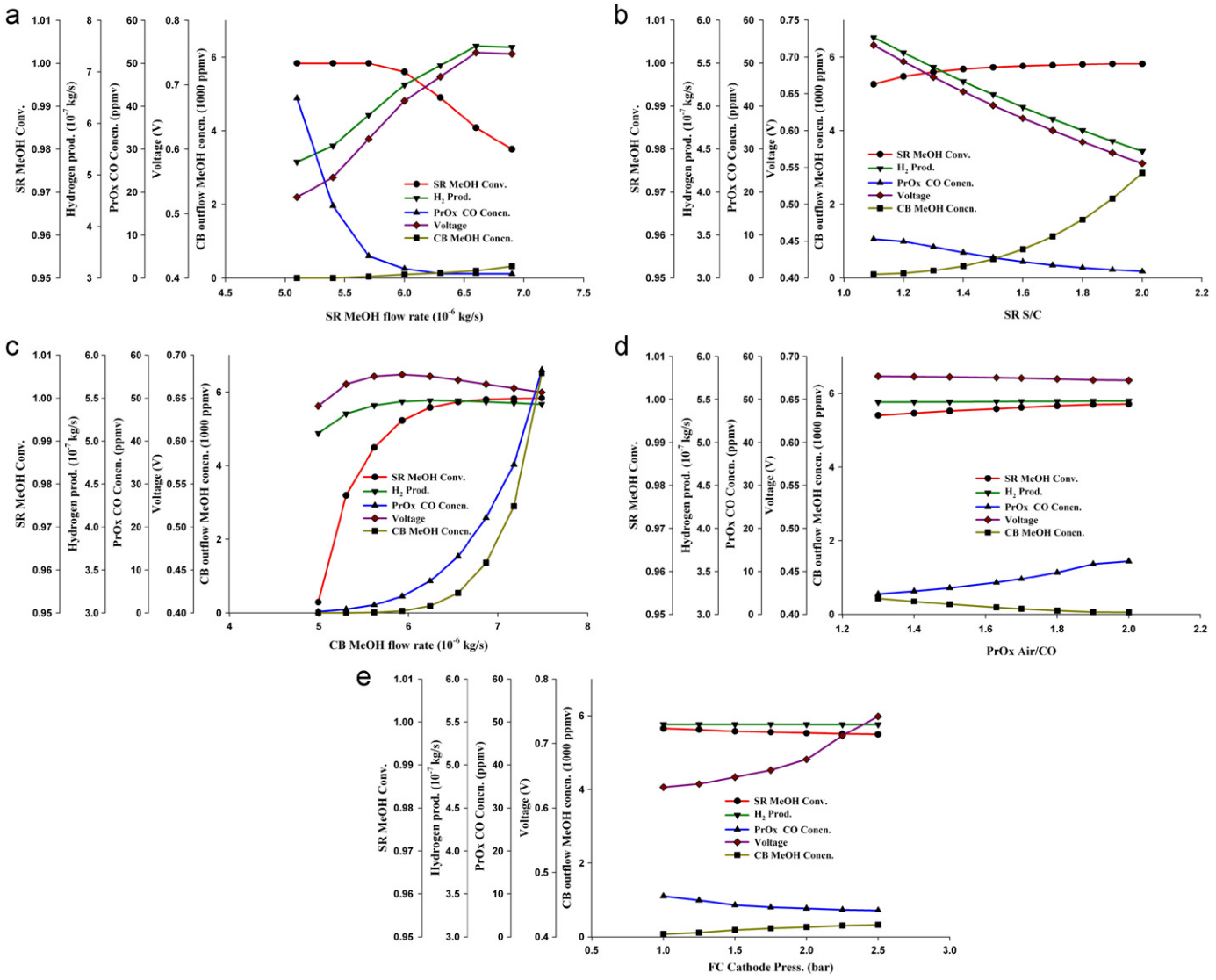

Fig. 4. Effects of operating conditions.

(P_{ca}). A sensitivity analysis reveals that P_{ca} is the major variable having influence on the fuel cell performance. The effects of these operating conditions on the above mentioned five performance indexes are summarized in Fig. 4. $F_{in,SR}$ significantly affects all the performance indexes, except $C_{MeOH,CB}$. $(S/C)_{SR}$ gives considerable impact on $C_{MeOH,CB}$ and V_{FC}. The effects of $F_{in,CB}$ on X_{SR}, C_{CO} and

$C_{MeOH,CB}$ are also noteworthy. The influences of $(O_2/CO)_{PrOx}$ and P_{ca} are relatively minor and that of $(A/C)_{CB}$ are negligible. These results shed light on selecting appropriate manipulated variables for the process control structure.

4. Process control structures

For micro chemical systems, control strategy is one of the most crucial challenges but only very few literature can be found. Shin and Besser (2007) conducted experimental study for a methanol micro steam reformer with build-in sensors and actuators using PID feedback control algorithm. Kolb et al. (2011) proposed a control structure for the start-up and normal operation of a micro ethanol fuel processor. The control strategy used feedback control of temperature, mass flow rate and pressure for major process units. For integrated FP/FC systems, studies of control strategy can be found only for conventional macro systems. One key feature needed is how the FP reacts to the load change from FC. Tsourapas et al. (2007) developed a feedforward plus feedback control scheme for a macro scale FP/FC system, where the feedforward control is for meeting the FC load change with maximum energy efficiency and the feedback control is for fast reacting to the change. Based on this concept, this study proposes several control structures and examines their performances using the dynamic model.

For control purpose, the input flow rates of two fuel streams to SR and CB should vary for given FC power requirement. Using the mathematical model, the optimal flow rates for maximum overall system energy efficiency can be determined. The efficiency is defined as the ratio of power output from fuel cell and the fuel input energy to the FP system as Eq. (1). The optimization analysis is accomplished utilizing the FEASOPT (feasible path successive quadratic programming optimizer) solver available in Aspen Custom Modeler®. The relationships between the voltage output and fuel input flow rates to the FP system obtained are listed in Eqs. (2) and (3) and shown in Fig. 5. The relationships of the two fuel inputs are reversed in direction. When the power output is raised, the optimal fuel input to SR must be increased but the optimal fuel input to CB must be reduced

$$\eta_o = \frac{VI}{(W_{MeOH,SR} + W_{MeOH,CB})(\Delta H_{C,MeOH})} \quad (1)$$

$$F_{in,SR} = 5.074 \times 10^{-7} + 1.43 \times 10^{-5} V + 3.344 \times 10^{-7} V^2 \quad (2)$$

$$F_{in,CB} = 6.756 \times 10^{-5} - 0.0001259 V + 5.981 \times 10^{-5} V^2 \quad (3)$$

A feedforward control structure for the FP/FC system can be implemented with these two functions. When the power output requirement of FC is changed, the controller will adjust the fuel input flow rates accordingly. The responses of the system by simulation are shown in Fig. 6 for the demand of increasing or decreasing the power output. The fuel inlet flow rates of SR and CB responding to voltage change are opposite. When the voltage output is to be raised, the fuel inlet flow rate of CB must be reduced but that of SR must be increased. If these opposite-direction flow rate adjustments are actuated simultaneously, the

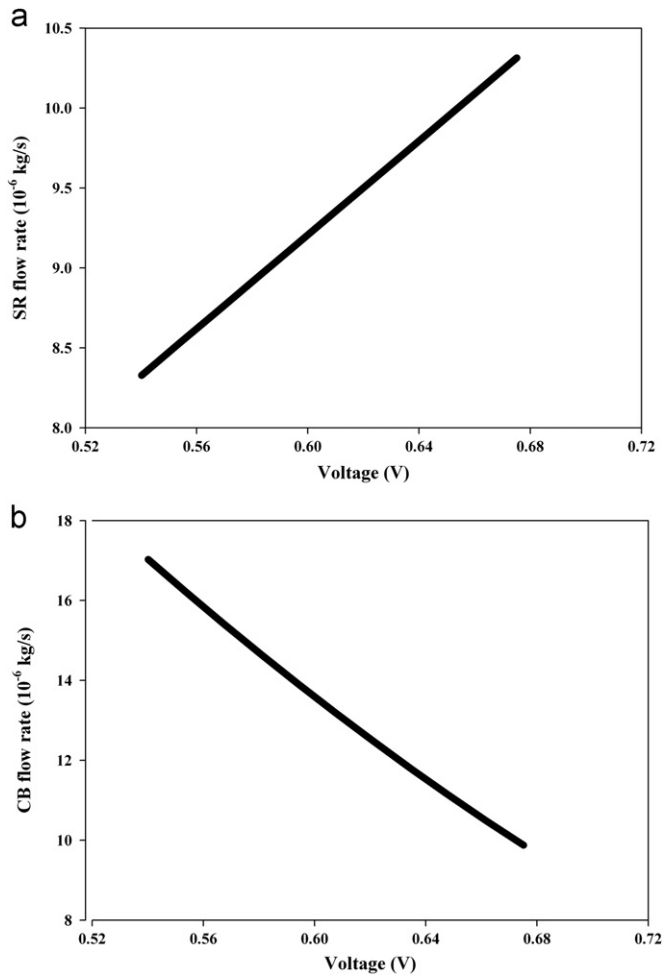

Fig. 5. Optimal fuel inlet flow rates.

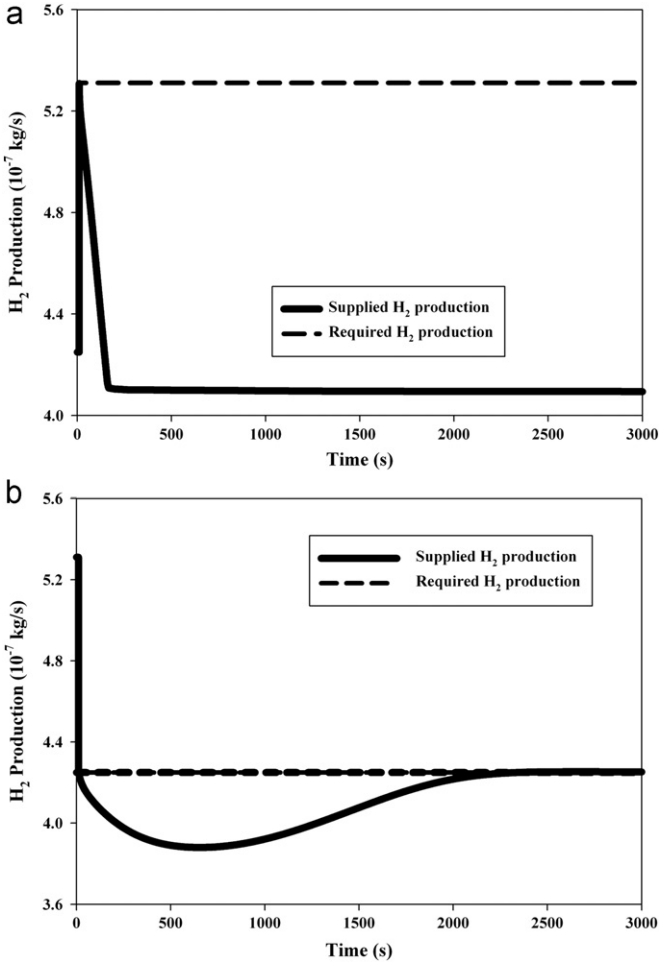

Fig. 6. Feedforward responses for voltage set-point change (a) 0.55 V→0.675 V and (b) 0.675 V→0.55 V.

temperature of SR will keep decreasing with time due to lower hydrogen supply to FC and return to CB. Thus, the target voltage change cannot be achieved. On the other hand, when the voltage output is to be lowered, the opposite-direction adjustments does not cause final deviation from the target, but it takes very long time to reach the new set point. The performances depicted in Fig. 6 clearly indicate that the simple feedforward control alone is an infeasible and ineffective strategy.

A hybrid feedforward and feedback control strategy is thus needed and three control structures are proposed and depicted in Fig. 7. The control structure 1 (CS1) uses double feedforward with double feedback control loops, which means the fuel inputs to SR

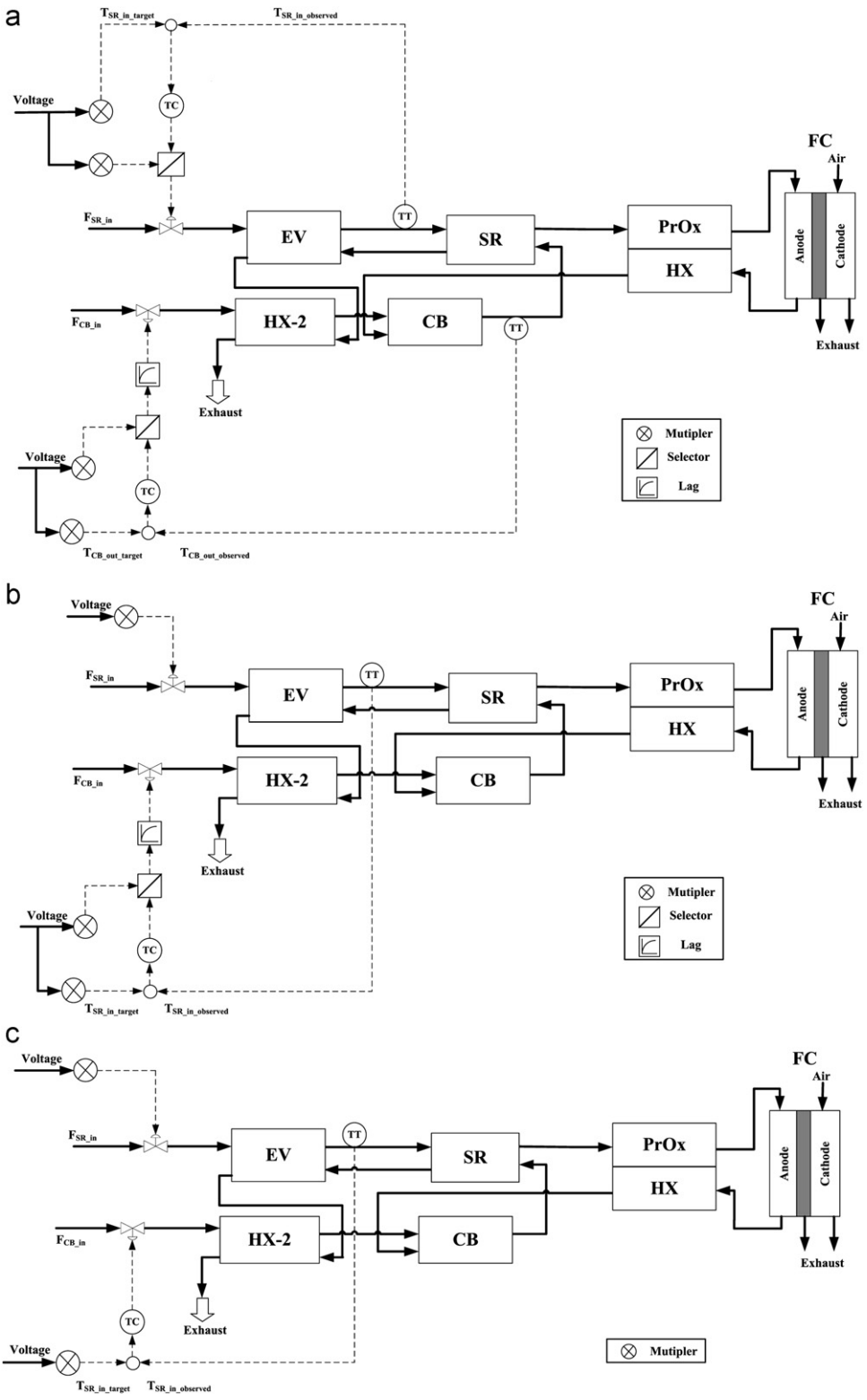

Fig. 7. Control structures (a) CS1—double feedforward with double feedback, (b) CS2—double feedforward with single feedback, (c) CS3—single feedforward with single feedback.

and CB are determined by the fore mentioned feedforword control and two feedback control loops are added to control the temperatures of SR inlet stream and CB outlet stream. These two controlled variables are chosen because they are the most significant operating conditions based on the conclusions from Section 3. The feedback controllers adjust the fuel inputs to SR and CB using PI algorithm to meet the temperature targets, which are the temperatures obtained via optimization for maximum energy efficiency. For the MIMO (multiple-input and multiple-output) feedback loops, relative gain array (RGA) is employed to determine the input–output pairing. The control structure 2 (CS2) uses double feedforward with single feedback control loops, which adopts only one feedback loop to control the temperature of SR inlet stream by manipulating the fuel input to CB. The control structure 3 (CS3) uses single feedforward with single feedback control loops, which applies feedforward control for the

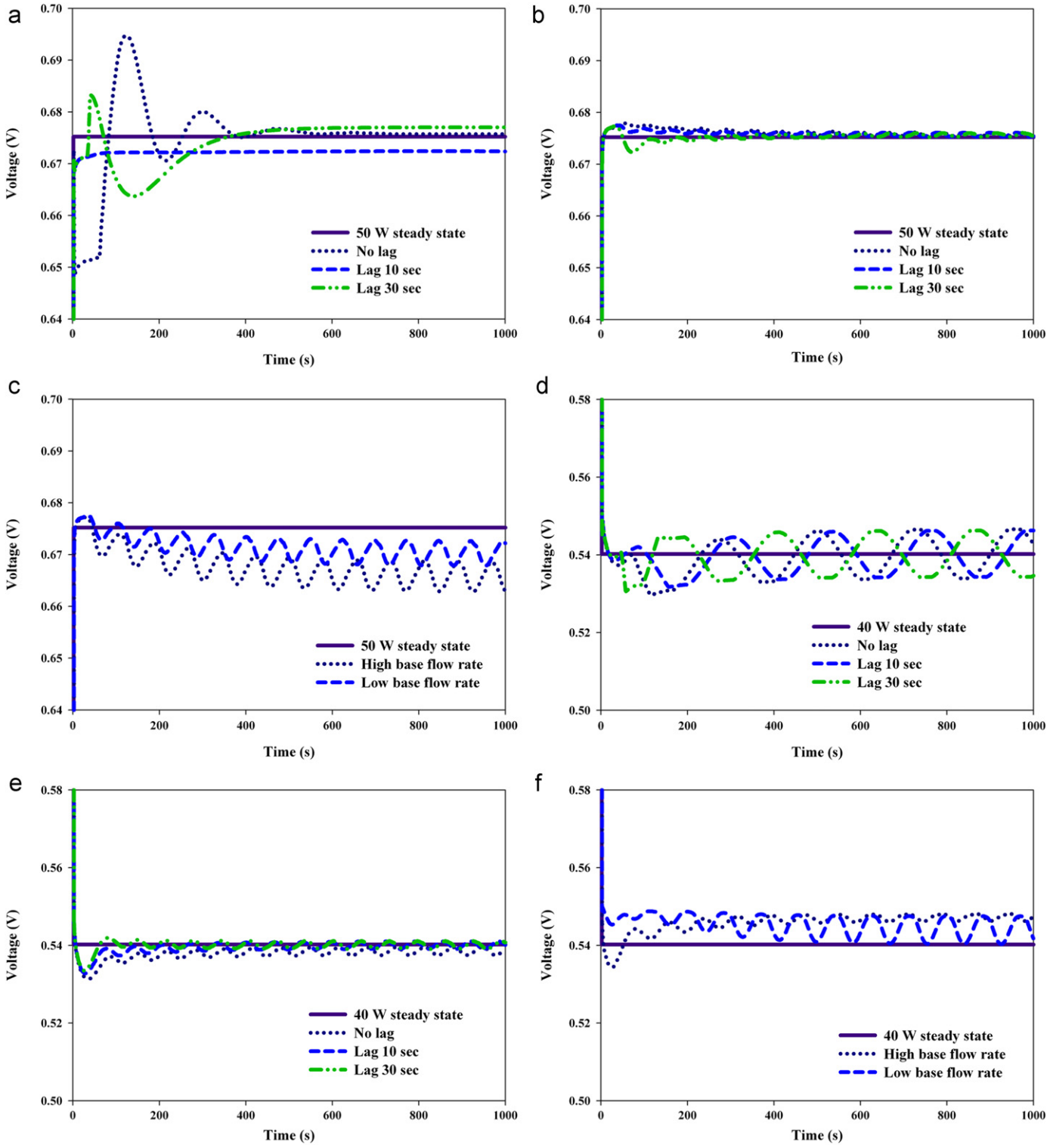

Fig. 8. Control performance for voltage set point change with Ziegler–Nichol tuning parameters: (a)–(c) for 0.55 V→0.675 V, (d)–(f) for 0.675 V→0.55 V. CS1: (a), (d). CS2: (b), (e). CS3: (c), (f).

fuel input to SR but not for the fuel input to CB and the feedback control paring, is the same as CS2. Because the fuel input to CB is not set by feedforward control, a base flow rate must be specified.

For each control structure, the parameters of PI controllers are determined by two approaches. First, the relay-feedback test and Ziegler–Nichol method (Luyben and Luyben, 1997) is used. Second, optimization analysis is used and the objective function to be minimized is the deviation of voltage ($\int |V(t)-V_{\text{target}}|dt$). Furthermore, to alleviate the unfavorable effect of simultaneous opposite-direction flow rate adjustments, a time lag is added in the CB fuel input control loop.

The performances of all the control structures with different parameter settings are summarized in Figs. 8 and 9. Out of all the alternatives, CS2 with Ziegler–Nichol tuning parameters and a lag of 30 s (CS2-ZN-30) gives the best response performance and is the best choice. Using the optimized PI controller parameters,

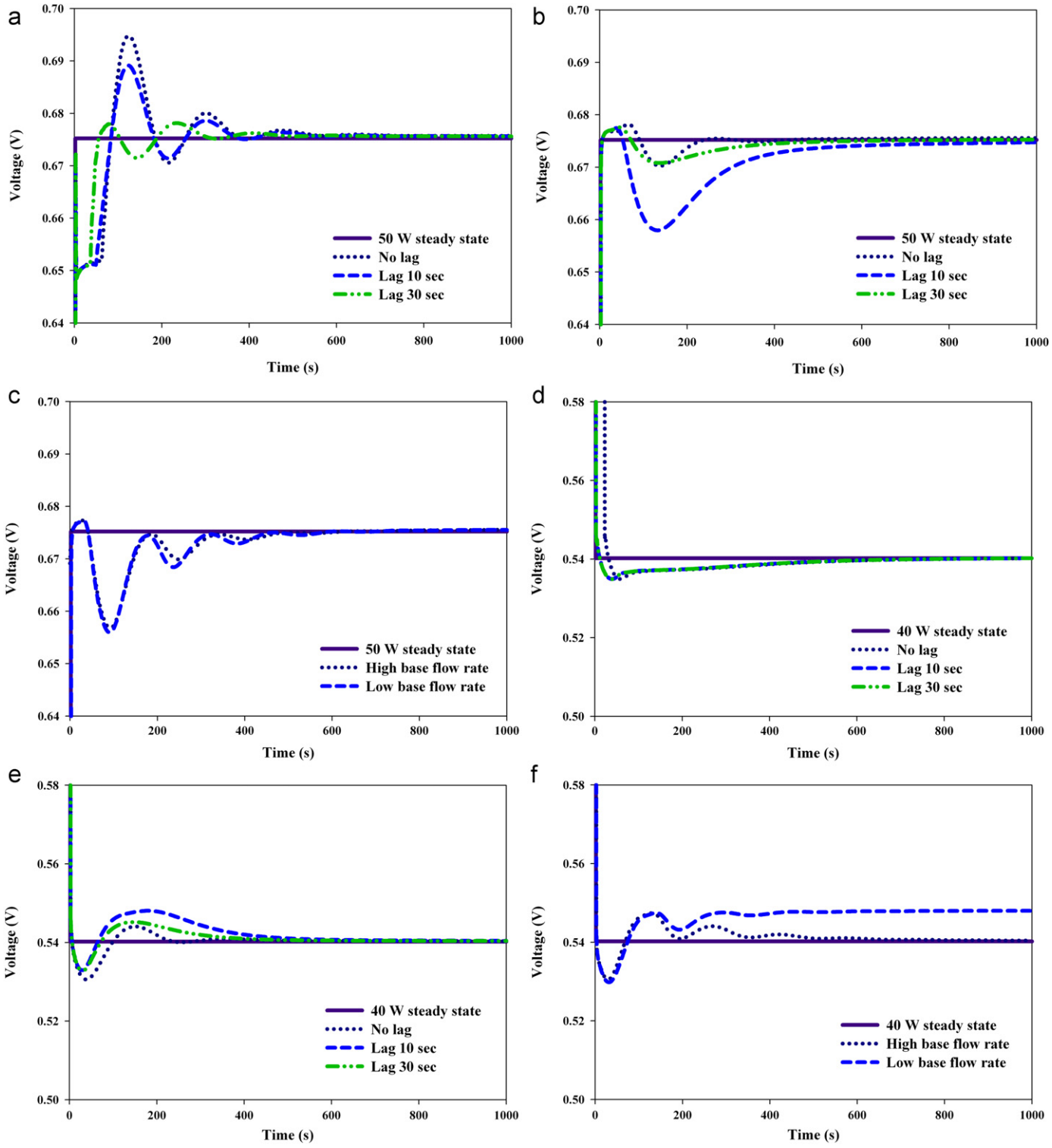

Fig. 9. Control performance for voltage set point change with optimized controller parameters: (a)–(c) for 0.55 V→0.675 V, (d)–(f) for 0.675 V→0.55 V. CS1: (a), (d). CS2: (b), (e). CS3: (c), (f).

improvements can be obtained for CS1 and CS3, but not for CS2. However, if the optimized PI controller parameters are used for CS2, the very small extent of fluctuation in response as seen in Fig. 8(b) and (e) can be eliminated. With the best choice, CS2-ZN-30, for responding voltage output increasing and decreasing, the initial damping periods are 120 and 60 s, the hydrogen shortage time periods are 64 and 58 s, and the extents of hydrogen shortage are 0.6 and 1.8%. The CO concentration, which is not shown in the figures, is always below 4 ppmv.

5. Conclusions

A dynamic mathematical model for an integrated methanol micro FP/FC process has been successfully developed and applied for investigating the design, performance and control of the process. The methanol micro fuel processor studied consists of the essential process units to supply high purity hydrogen with carbon dioxide concentration below 10 ppmv for the PEMFC, including evaporator, combustor, steam reforming, preferential oxidation and heat exchangers. The plate-fin type micro devices are adopted. The mathematical models for process units are one dimensional or zero dimensional, but the heat and mass transfer mechanisms as well as the reaction kinetics are taken into account. The flowsheet simulation with control functions has been successfully demonstrated on Aspen Custom Modeler® platform.

The steady state sensitivity analysis reveals that the significant operating conditions for the FP/FC process are the feed flow rate and steam/carbon ratio of the steam reformer and the feed flow rate of the combustor.

The dynamic simulation analysis allows for the comparison of different control schemes to respond for the voltage change demand of PEMFC. The simple feedforward control, which sets optimal feed flow rates for maximum energy efficiency operation, is infeasible and ineffective. Out of the three proposed control schemes, the structure using double feedforward with single feedback control loops (CS2), Ziegler–Nichol tuning parameter and 30 s time lag provides the best performance.

In the future, the fluid mechanics and the effects of BOP components, such as valves, pumps, sensors, actuators, etc., should be included in the modeling and analysis.

Notation

a	surface area per unit volume of reactor, m^2/m^3
A	cross section area of reactor, m^2
Cp	heat capacity, J/(kg-K)
CS	control structure
F	flow rate, kg/s
h	heat transfer coefficient, $W/(m^2\text{-}K)$
I	current density, A/cm^2
kc	thermal conductivity W/(m-K)
k	Mass transfer coefficient, m/s
L	length, m
M	mass flow rate, kg/s
Mw	molecular weight, kg/kmol
P	pressure, Pa
Q	heat flux, W/m^2
R	gas constant, J/(K-mole)
Rxn	reaction rate, kmol/(kg cat-s)
Sc	source term of mass, $kmol/(m^3\text{-}s)$
Se	source term of energy, $W/(m^3\text{-}s)$
T	temperature, K
u	internal energy, J/kg
V	volume, m^3 or voltage, V
W	width, m
X	flow rate reduction ratio
y	mass fraction
z	flow direction coordinate (m)

Greek letters

ΔH	enthalpy change, J/mol
ε	volume fraction of the reactor
η	efficiency
ρ	density, kg/m^3
υ	stoichiometric coefficient

Subscripts

1	liquid zone
2	two phase zone
3	superheated vapor zone
an	anode
avg	average
bulk	bulk
c	channel
C	cold
cat	catalyst
CB	combustor
CS	cold side fluid
EV	evaporator
ex	external
FC	fuel cell
g	gas
H	hot
HS	hot side fluid
HX	heat exchanger
i	species i
in	inlet
int	interface
L	liquid
LV	liquid–vapor two phase zone
m	manifold
m_c	manifold extended zone
out	outlet
PrOx	preferential oxidation reactor
s	solid
SL	saturated liquid
SR	steam reformer
T	total
v	vapor
w	wall
wc	wall with catalyst

Acknowledgment

The authors gratefully acknowledge the sponsorship from the National Science Council of Taiwan (NSC-99-2221-E-032-061-MY2).

Appendix A. Mathematical model for reactor

A one dimensional model for the micro reactor is described in the following. Mass and energy balance equations are derived for

the bulk gas, solid wall with catalyst layer and solid wall without catalyst layer, respectively.

For each species i in the bulk gas, the mass balance considers the inlet and outlet flows as well as the mass transfer from the bulk gas-catalyst interface. The bulk gas follows ideal gas law

$$\varepsilon_g \frac{\partial(\rho_{g,\mathrm{bulk}} y_{g,i})}{\partial t} = -\frac{1}{A}\frac{\partial(M_g y_{g,i})}{\partial z} + k_{g,i}\rho_{g,\mathrm{bulk}} a_{\mathrm{wc},g}(y_{\mathrm{int},i} - y_{g,i}) \tag{A1}$$

$$\rho_{g,\mathrm{bulk}} = \frac{P\sum_i y_{g,i}\mathrm{Mw}_i}{RT_g} \tag{A2}$$

For each gas species i inside the catalyst layer, the mass balance takes into account the mass transfer to the bulk gas as well as all the chemical reactions associated to the species. The gas inside the catalyst layer follows ideal gas law

$$\varepsilon_{\mathrm{wc}} \frac{\partial(\rho_{g,\mathrm{cat}} y_{s,i})}{\partial t} = -k_{s,i}\rho_{g,\mathrm{cat}} a_{\mathrm{wc},g}(y_{s,i} - y_{\mathrm{int},i}) + \mathrm{Mw}_i \mathrm{Sc}_i \tag{A3}$$

$$\mathrm{Sc}_i = \rho_{g,\mathrm{cat}}\varepsilon_{\mathrm{cat}} \sum_j \nu_{ij}\mathrm{Rxn}_{s,j} \tag{A4}$$

$$\rho_{g,\mathrm{cat}} = \frac{P\sum_i y_{s,i}\mathrm{Mw}_i}{RT_{g,\mathrm{cat}}} \tag{A5}$$

At the inlet of the reactor, the concentrations of bulk gas, bulk gas-catalyst interface and catalyst layer are assumed to be equal. On both sides of the bulk gas-catalyst interface, the mass fluxes are equal

$$y_{g,i}(0,t) = y_{\mathrm{int},i}(0,t) = y_{s,i}(0,t) \tag{A6}$$

$$k_{g,i}\rho_{g,\mathrm{bulk}}(y_{\mathrm{int},i} - y_{g,i}) = k_{s,i}\rho_{g,\mathrm{cat}}(y_{s,i} - y_{\mathrm{int},i}) \tag{A7}$$

The energy balance of bulk gas involves the energy flows due to gas flows as well as the heat transfers across the interfaces of bulk gas–solid walls with or without catalyst layers

$$\varepsilon_g \frac{\partial(\rho_{g,\mathrm{bulk}}\mathrm{Cp}_{g,\mathrm{bulk}} T_g)}{\partial t} = -\frac{1}{A}\frac{\partial(M_g \mathrm{Cp}_{g,\mathrm{bulk}} T_g)}{\partial z} - h_{sg} a_{\mathrm{wc},g}(T_g - T_{\mathrm{wc}}) - h_{sg} a_{w,g}(T_g - T_w) \tag{A8}$$

For the solid wall with catalyst layer, the energy balance considers the heat conduction in the z-direction (gas flow direction), the heat transfer across the bulk gas–solid wall and the energy effects from chemical reactions

$$E_{\mathrm{wc}}\rho_w \mathrm{Cp}_w \frac{\partial T_{\mathrm{wc}}}{\partial t} = \varepsilon_{\mathrm{wc}}\mathrm{kc}_w \frac{\partial^2 T_{\mathrm{wc}}}{\partial z^2} + h_{sg} a_{\mathrm{wc},g}(T_g - T_{\mathrm{wc}}) + \mathrm{Se} \tag{A9}$$

$$\mathrm{Se} = -\rho_{g,\mathrm{cat}}\varepsilon_{\mathrm{cat}} \sum_j \Delta H_j \mathrm{Rxn}_{s,j} \tag{A10}$$

The energy balance of the solid wall without catalyst layer considers the heat conduction in the z-direction and the heat transfer across the bulk gas–solid wall

$$\varepsilon_w \rho_w \mathrm{Cp}_w \frac{\partial T_w}{\partial t} = \varepsilon_w \mathrm{kc}_w \frac{\partial^2 T_w}{\partial z^2} + h_{sg} a_{w,g}(T_g - T_w) \tag{A11}$$

At the inlet of the reactor, the temperatures of bulk gas, bulk gas-catalyst interface and catalyst layer are assumed to be equal. For the solid walls, the heat fluxes in the z-direction at the reactor inlet and outlet are zero

$$T_g(0,t) = T_{\mathrm{wc}}(0,t) = T_w(0,t) \tag{A12}$$

$$\left.\frac{\partial T_{\mathrm{wc}}(z,t)}{\partial z}\right|_{z=0} = \left.\frac{\partial T_{\mathrm{wc}}(z,t)}{\partial z}\right|_{z=L} = \left.\frac{\partial T_w(z,t)}{\partial z}\right|_{z=0} = \left.\frac{\partial T_w(z,t)}{\partial z}\right|_{z=L} = 0. \tag{A13}$$

Appendix B. Mathematical model for heat exchanger with phase change

For the heat exchanger with phase change, the zero dimensional model is explained in the following.

For the cold fluid side, where evaporation occurs, the heat exchanger is divided into three zones, including the liquid, two phase and superheated vapor. The mass balances for the three zones are given in Eqs. (A14)–(A16). The change of liquid volume in the cold fluid two phase zone can be expressed in terms of the change of liquid mass flow rate. In the equations, M_{LV} is the mass flow rate of vaporized fluid

$$M_{\mathrm{CS,in}} - M_{\mathrm{SL,out}} = 0 \tag{A14}$$

$$\rho_L \frac{dV_2}{dt} = M_{\mathrm{SL,out}} - M_{\mathrm{LV}} \tag{A15}$$

$$M_{\mathrm{LV}} - M_{\mathrm{CS,out}} = 0 \tag{A16}$$

The energy balances for the cold fluid are expressed for the three zones as Eqs. (A17)–(A19). The heat fluxes across the walls of the three zones are Q_1, Q_2 and Q_3. For the two phase zone, the heat of vaporization is accounted for as given in Eq. (A18)

$$M_{\mathrm{CS,in}}\mathrm{Cp}_{\mathrm{CS},L}(T_{\mathrm{CS,in}} - T_{\mathrm{CS,sat}}) + Q_1 = 0 \tag{A17}$$

$$\rho_{\mathrm{CS}} u_{\mathrm{CS}} \frac{dV_2}{dt} = M_{\mathrm{SL,out}} H_{\mathrm{SL,out}} - M_{\mathrm{LV}} H_{\mathrm{LV}} + Q_2 \tag{A18}$$

$$M_{\mathrm{CS,in}}\mathrm{Cp}_{\mathrm{CS},V}(T_{\mathrm{CS,out}} - T_{\mathrm{CS,sat}}) + Q_3 = 0 \tag{A19}$$

For the hot fluid side, no phase change occurs, the mass and energy balances are written for the entire heat exchanger

$$M_{\mathrm{HS,in}} - M_{\mathrm{HS,out}} = 0 \tag{A20}$$

$$M_{\mathrm{HS,in}}\mathrm{Cp}_{\mathrm{HS}}(T_{\mathrm{HS},1} - T_{\mathrm{HS,out}}) - Q_1 = 0 \tag{A21}$$

$$M_{\mathrm{HS,in}}\mathrm{Cp}_{\mathrm{HS}}(T_{\mathrm{HS},2} - T_{\mathrm{HS},1}) - Q_2 = 0 \tag{A22}$$

$$M_{\mathrm{HS,in}}\mathrm{Cp}_{\mathrm{HS}}(T_{\mathrm{HS,in}} - T_{\mathrm{HS},2}) - Q_3 = 0 \tag{A23}$$

For the heat exchanger, each interface heat flux can be expressed in terms of the relations for cold fluid, solid wall and hot fluid

$$Q_1 = h_{W,1}V_1 a(T_{\mathrm{WH1}} - T_{\mathrm{WC1}}) = h_{\mathrm{CS},1}V_1 a(T_{\mathrm{WC1}} - T_{\mathrm{CS,avg1}}) = h_{\mathrm{HS},1}V_1 a(T_{\mathrm{HS,avg1}} - T_{\mathrm{WH1}}) \tag{A24}$$

$$Q_2 = h_{W,2}V_2 a(T_{\mathrm{WH2}} - T_{\mathrm{WC2}}) = h_{\mathrm{CS},2}V_2 a(T_{\mathrm{WC2}} - T_{\mathrm{CS,avg2}}) = h_{\mathrm{HS},2}V_2 a(T_{\mathrm{HS,avg2}} - T_{\mathrm{WH2}}) \tag{A25}$$

$$Q_3 = h_{W,3}V_3 a(T_{\mathrm{WH3}} - T_{\mathrm{WC3}}) = h_{\mathrm{CS},3}V_3 a(T_{\mathrm{WC3}} - T_{\mathrm{CS,avg3}}) = h_{\mathrm{HS},3}V_3 a(T_{\mathrm{HS,avg3}} - T_{\mathrm{WH3}}) \tag{A26}$$

The volumes of the three zones must meet the total volume constraint

$$V_T = V_1 + V_2 + V_3. \tag{A27}$$

References

Arzamendi, G., Diéguez, P.M., Montes, M., Centeno, M.A., Odriozola, J.A., Gand, L.M., 2009. Integration of methanol steam reforming and combustion in a microchannel reactor for H_2 production: a CFD simulation study. Catal. Today 143, 25.

Bard, A.J., Faulkner, L.R., 2001. Electrochemical Methods—Fundamentals and Applications. John Wiley and Sons, Inc., N.Y.

Chen, F., Chang, M.H., Kuo, C.Y., Hsueh, C.Y., Yan, W.M., 2009. Analysis of a plate-type microreformer for methanol steam reforming reaction. Energy Fuels 23, 5092.

Choi, Y., Stenger, H.G., 2004. Kinetics, simulation and insights for CO selective oxidation in fuel cell applications. J. Power Sources 129, 246.

Delsman, E.R., de Croon, M.H.J.M., Kramer, G.J., Cobden, P.D., Hofmann, C., Cominos, V., Schouten, J.C., 2004. Experiments and modeling of an integrated preferential oxidation-heat exchanger microdevice. Chem. Eng. J. 101, 123.

Delsman, E.R., Laarhoven, J.P.F., de Croon, M.H.J.M., Kramer, G.J., Schouten, J.C., 2005. Comparison between conventional fixed-bed and microreactor technology for a portable hydrogen production case. Chem. Eng. Res. Des. 83, 1063.

Golbert, J., Lewin, D.R., 2004. Model-based control of fuel cells: (1) regulatory control. J. Power Sources 135, 135.

Kolb, G., Schürer, J., Tiemann, D., Wichert, M., Zapf, R., Hessel, V., Löwe, H., 2007. Fuel processing in integrated micro-structured heat-exchanger reactors. J. Power Sources 171, 198.

Kolb, G., Schelhaas, K.-P., Wichert, M., Burfeind, J., Hesske, C., Bandlamudi, G., 2009. Development of a microstructured methanol fuel processor coupled to a high temperature PEM fuel cell. Chem. Eng. Technol. 32, 1739.

Kolb, G., Men, Y., Schelhaas, K.P., Tiemann, D., Zapf, R., Wilhelm, J., 2011. Development work on a microstructured 50 kW ethanol fuel processor for a small scale stationary hydrogen supply system. Ind. Eng. Chem. Res. 50, 2554.

Korotkikh, O., Farrauto, R., 2000. Selective catalytic oxidation of CO in H2: fuel cell applications. Catal. Today 62, 249.

Llopis, R., Cabello, R., Navarro-Esbrí, J., Torrella, E., 2007. A dynamic mathematical model of a shell-and-tube evaporator. Int. J. Energy Res. 31, 232.

Luyben, W., Luyben, M., 1997. Essentials of Process Control. McGraw-Hill.

Men, Y., Kolb, G., Zapf, R., Tiemann, D., Wichert, M., Hessel, V., Löwe, H., 2008. A complete miniaturised microstructured methanol fuel processor/fuel cell system for low power applications. Int. J. Hydrogen Energy 33, 1374.

Morse, J.D., Upadhye, R.S., Graff, R.T., Spadaccini, C., Park., H.G., Hart, E.K., 2007. A MEMS-based reformed methanol fuel cell for portable power. J. Micromech. Microeng. 17, 237.

Park, G.G., Seo, D.J., Park, S.H., Yoon, Y.G., Kim, C.S., Yoon, W.L., 2004. Development of microchannel methanol steam reformer. Chem. Eng. J. 101, 87.

Pasel, J., Emonts, B., Peters, R., Stolten, D., 2001. A structured test reactor for the evaporation of methanol on the basis of a catalytic combustion. Catal. Today 69, 193.

Peppley, B.A., Amphlett, J.C., Kearns, L.M., Mann, R.F., 1999. Methanol-steam reforming on $Cu/ZnO/Al_2O_3$ catalysts. Part 2. A comprehensive kinetic model. Appl. Catal. A: Gen. 179, 31.

Shah, K., Ouyang, X., Besser, R.S., 2005. Microreaction for microfuel processing: challenges and prospects. Chem. Eng. Technol. 28, 303.

Shin, W.C., Besser, R.S., 2007. Toward autonomous control of microreactor system for steam reforming of methanol. J. Power Sources 164, 328.

Sohn, J.M., Byun, Y.C., Cho, J.Y., Choe, J., Song, K.H., 2007. Development of the integrated methanol fuel processor using micro-channel patterned devices and its performance for steam reforming of methanol. Int. J. Hydrogen Energy 32, 5103.

Terazaki, T., Nomura, M., Takeyama, K., Nakamura, O., Yamamoto, T., 2005. Development of multi-layered microreactor with methanol reformer for small PEMFC. J. Power Sources 145, 691.

Tsourapas, V., Stefanopoulou, A.G., Sun, J., 2007. Model-based control of an integrated fuel cell and fuel processor with exhaust heat recirculation. IEEE Trans. Control Syst. Technol. 15, 233.

US DOE (Department of Energy), Fuel Cell Handbook, fifth ed., October 2000.

Vahabi, M., Akbari, M.H., 2009. Three-dimensional simulation and optimization of an isothermal PROX microreactor for fuel cell applications. Int. J. Hydrogen Energy 34, 1531.

Won, J.Y., Jun, H.K., Jeon, M.,.K., Woo, S.I., 2006. Performance of microchannel reactor combined with combustor for methanol steam reforming. Catal. Today 111, 158.

Yoshida, K., Tanaka, S., Hiraki, H., Esashi, M., 2006. A micro fuel reformer integrated with a combustor and a microchannel evaporator. J. Micromech. Microeng. 16, S191.